Int. J. of Geosynth. and Ground Eng. (2017) 3:2
DOI 10.1007/s40891-016-0078-y

ORIGINAL ARTICLE

A Numerical Procedure for the Assessment of Contact Pressures on Buried Structures Overlain by EPS Geofoam Inclusion

M. A. Meguid[1] · **M. G. Hussein**[1]

Received: 28 September 2016 / Accepted: 3 December 2016

Abstract Extruded Polystyrene (EPS) geofoam is a light weight material used in a wide range of geotechnical engineering applications including embankment construction and bridge approaches to reduce earth loads imposed on the adjacent or underlying soils and structures. EPS is also used as a compressible material above deeply buried culverts to promote positive arching and reduce the load transferred to the walls of the structure. An important step towards understanding the soil-geofoam-structure interaction and accurately model the load transfer mechanism is choosing a suitable material model for the EPS geofoam that is capable of simulating the material response to compressive loading for various ranges of strains. In this study, a material model that is able to capture the response of EPS geofoam is first established and validated using index test results for three different geofoam materials. To examine the performance of the model in analyzing complex interaction problems, a laboratory experiment that involves a rigid structure buried in granular material with EPS geofoam inclusion is simulated. The contact pressures acting on the walls of the structure are calculated and compared with measured data for three different geofoam materials. The developed numerical model is then used to study the role of geofoam density on the earth loads acting on the buried structure. Significant pressure reduction is achieved using EPS15 with a pressure ratio of 0.28 of the theoretical overburden pressure at the upper wall. The proposed FE modeling approach is found to be efficient in capturing the behavior of EPS geofoam material under complex interaction soil-structure condition.

Keywords Finite element method · EPS geofoam · Buried structures · Soil-structure interaction · Soil arching

Introduction

Earth loads on buried conduits are known to be dependent on the installation conditions. A conduit installed in a trench is usually located completely below the natural ground surface and frictional forces between the sides of the trench and the backfill material help to partially support the weight of the overlaying soil. Embankment installation, however, refers to the condition when soil is placed in layers above the natural ground. The vertical earth pressure on a rigid conduit installed using embankment construction method is generally greater than the weight of the soil above the structure because of negative arching. The induced trench installation (also called imperfect ditch or ITI method) has been often used to reduce vertical earth pressure on rigid conduits. The method involves installing a compressible layer immediately above the conduit to generate positive arching in the overlying soil. The Canadian highway bridge design code [1] and the AASHTO LRFD bridge design specifications [2] provide guidelines for estimating earth loads on positive projecting culverts, but not for culverts installed using induced trench technique. This construction method has been an option used by designers to reduce earth pressures on rigid conduits buried under high embankments. Despite its obvious benefits, recent

✉ M. A. Meguid
mohamed.meguid@mcgill.ca

M. G. Hussein
mahmoud.hussein3@mail.mcgill.ca

[1] Civil Engineering and Applied Mechanics, McGill University, 817 Sherbrooke St. W., Montreal, QC H3A 0C3, Canada

doubts have left many designers uncertain as to the viability of induced trench construction [3].

The ITI method of installing rigid conduits under high embankments dates back to the early 1900s. Researchers studied the relevant soil-structure interaction using experimental testing or field instrumentation [4–8], as well as numerical modelling [9–13] to help understand the method and address uncertainties associated with this design approach.

EPS geofoam material is known to compress in response to uniaxial compression loading without apparent shear failure and, therefore, it is difficult to establish the failure state of the material [14]. It has been accepted in design to use parameters (e.g. elastic limit and initial tangent modulus) that are obtained from the linear elastic stress–strain behavior at 1% strain measured in a monotonic compression load test. Significant efforts have been made by researchers to model the short-term behavior of EPS geofoam used in geotechnical engineering projects. The material is often approximated as linear elastic-perfectly plastic (e.g. [15]) or nonlinear elasto-plastic material (e.g. [16]). Other nonlinear models have been proposed to capture the material response under triaxial loading (e.g. [17–19]).

It is often desired to use index test data (e.g. [20]), routinely conducted by the manufacturer, to create a representative material model that can be implemented directly into a finite element analysis and used to simulate the compressive behavior of EPS geofoam in a given application.

Scope The objective of this study is to propose a numerical modeling procedure that can be used to investigate soil arching associated with induced trench installation of rigid conduits overlain by EPS geofoam inclusions. A nonlinear elastic–plastic hardening model is first established for three different EPS geofoam densities. The model takes advantage of the standard compression tests usually performed by the manufacturer to extract essential plasticity data that allows for the behavior to be numerically simulated. The developed model is further used to examine the role of EPS geofoam density in reducing the earth pressures exerted on a rigid buried structure.

The finite element (FE) analyses presented throughout this investigation have been performed using the general finite element software ABAQUS/Standard, version 6.13 [21]. It should be noted that the rheological and anisotropic aspects of EPS geofoam were not addressed in this study.

EPS Material Model

Three types of EPS geofoam materials, namely: (1) EPS15; (2) EPS22; and (3) EPS39, are modeled in this study. Index test results obtained from a series of uniaxial unconfined compression tests, carried out by the manufacturer, are presented in Fig. 1. The tests were performed on 125 mm cubes under monotonic loading for the three different EPS types. Results show that the tested EPS geofoam generally behaves as a nonlinear elasto-plastic hardening material. A constitutive model that is capable of describing the details of material behavior, including the nonlinearity, elasticity, isotropic hardening and plasticity, is needed. These components have been combined using the commercial finite element software ABAQUS and used to represent the EPS geofoam material throughout this study. The approach used to combine these model features is based on the conversion of the measured strains and stresses into the appropriate input parameters in ABAQUS. This is achieved by decomposing the total strain values into elastic and plastic strains to cover the entire range of the EPS response.

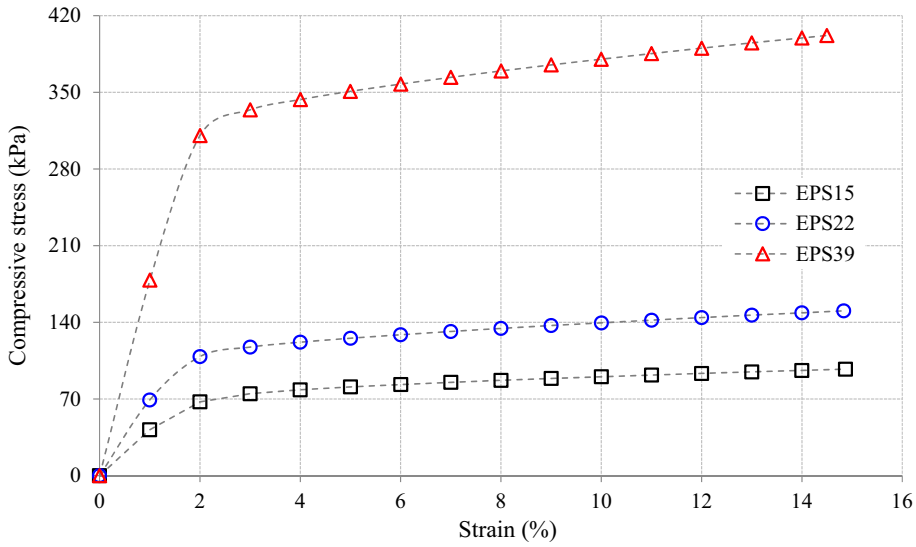

Fig. 1 Compression test results for three different EPS geofoam materials

Model Components

The elasticity component of the EPS model is described by an elastic isotropic model where the total stress and the total strain are related using the elasticity matrix. The plasticity is modeled using Mises yield criterion with isotropic hardening and associated flow rule. The isotropic yielding is defined by expressing the uniaxial compressive yield stress as a function of the equivalent uniaxial plastic strain. The isotropic hardening rule is expressed in ABAQUS using a tabular data of compressive yield stress as a function of plastic strains.

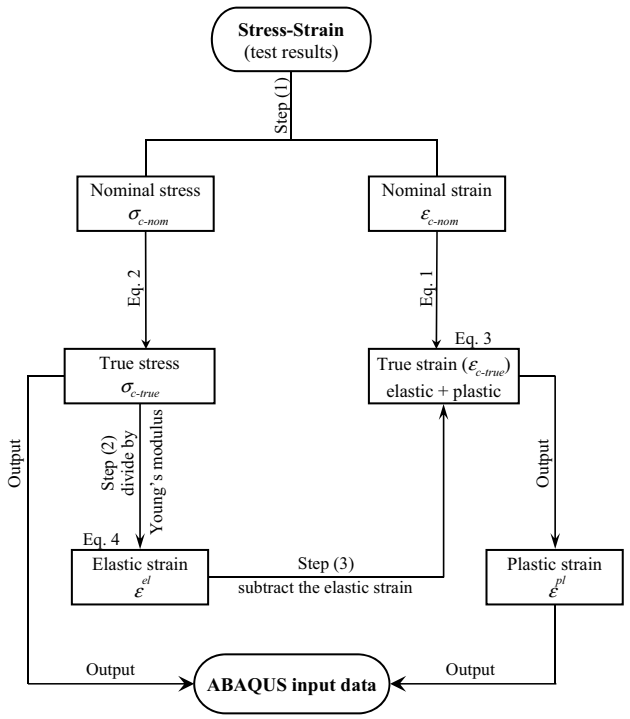

Fig. 2 Procedure used to generate ABAQUS input parameters for the EPS geofoam

The plasticity data has to be specified in terms of true stresses and true strains despite the fact that test data provides nominal (engineering) values of total stresses and total strains [21]. A procedure is, therefore, needed to first convert the nominal test data into its true values and then decompose the total strain values into elastic and plastic strain components to allow for direct data input into ABAQUS. A flow chart that illustrates the procedure adopted to determine the numerical input data based on the experimental results is given in Fig. 2 and summarized in the following steps:

1. Converting the test data (stresses and strains) from nominal to true values using:

$$e_{c\ true} = \ln(1 + e_{c\ nom}) \tag{1}$$

$$\sigma_{c\ true} = \frac{\sigma_{cnom}}{(1 - \nu \cdot \varepsilon_{c\ nom})^2} \tag{2}$$

where ν is the EPS Poissons ratio

$$e_{c\ true} = e^{el} + e^{pl} \tag{3}$$

2. Using the true stress (σ_{true}) and Young's modulus (E) to obtain the elastic strain component:

$$e^{el} = s_{true}/E \tag{4}$$

3. Subtracting the elastic strain values from the total true strains to determine plastic strains.

Then, decomposing the total true strain ($\varepsilon_{c\ true}$) into elastic and plastic components as illustrated in Fig. 3a:

The final EPS plasticity properties are introduced into ABAQUS input module in terms of true stresses versus plastic strains. It should be noted that the compressive stresses and strains used in the above procedure are negative values.

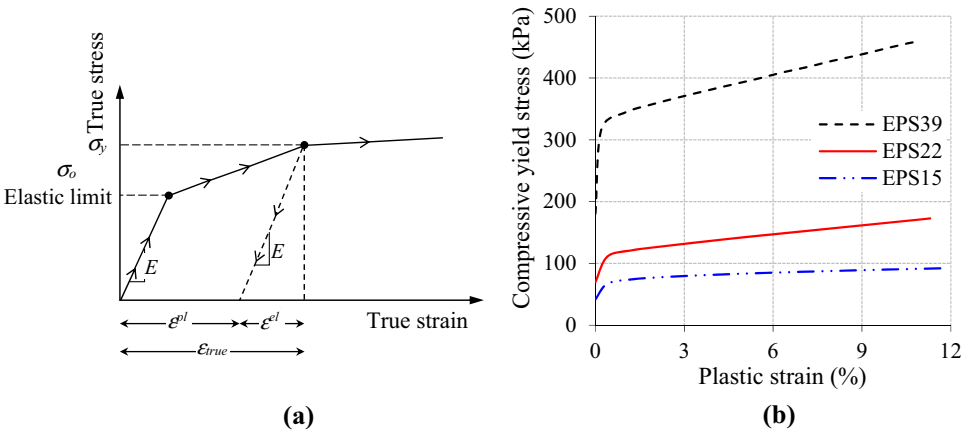

Fig. 3 EPS plasticity model: **a** decomposition of the total true strain, **b** hardening rule

The Young's modulus used to describe the EPS elasticity model is determined using the initial true stress and strain values. Discrepancy of the Poisson's ratio value for EPS geofoam was found in the literature. Most frequently, values range between 0.05 and 0.2 were used. Recent research conducted by Negussey [22] concluded that a Poisson's ratio value of 0.1 is appropriate. The elastic properties for the three EPS types used in the numerical study are summarized in Table 1. The hardening rule data used to describe the EPS plasticity model is shown in Fig. 3b.

Modeling the Compression Test

Three-dimensional FE analyses are conducted to simulate the EPS compressive tests on 125 mm cubes. The elasto-plastic constitutive model, described above, is used to simulate the measured behavior of the EPS. The cube geometry is discretized using 8-node linear brick elements (C3D8) with eight integration points. To simulate the uniaxial compressive test, the EPS model is restrained in the vertical direction ($U_z = 0$) along the base and a compressive load is applied at the top using a prescribed velocity (V_z). The cube movements are constrained in X and Y directions at both ends (top and bottom) to simulate the friction between the grips of the loading machine and the EPS cube. The 3D FE mesh used in the analysis, with over 74,000 elements, is shown in Fig. 4. Several mesh sizes were tested to determine a suitable mesh that brings a balance between accuracy and computing cost. An average element size of 3 mm was found to satisfy the balance and produce accurate results.

To validate the numerical model, the calculated and measured load–strain relationships are compared in Fig. 5. It can be seen that the calculated responses for EPS15 and EPS22 agree well with the measured data. For EPS39, the model slightly overestimated the compressive resistance beyond the yield point. In general, the proposed elasto-plastic constitutive model was found to reasonably represent the response of the material in both the elastic and plastic regions.

The results also confirm that there is no obvious shear failure of the material up to 18% strain. For design purposes, the 1, 5, and 10% strains are often used to limit the applied pressure, depending on the nature of the project. Figure 6 illustrate the normal stress distributions within the EPS cube at 5% strain level for the three densities used in this study. It is noted that the maximum compressive stress was found to be located near the top and bottom sides of the cube and the stress decreased towards the middle. At 5% strain, stresses developing at the center of the blocks increased from 70 kPa for EPS15 (Fig. 6a) to 100 kPa for EPS22 (Fig. 6b) and reached about 300 kPa for EPS39 (Fig. 6c). The stresses developing in EPS15 and EPS22 were found to be about 20 and 35%, respectively, of that calculated for EPS39. This attributed to the fact that EPS39 (the stiffer of the three investigated materials) would require higher applied pressure to reach 5% strain as compared to EPS 15 and EPS22.

Effect of Lateral Confinement

The effect of confinement pressure on the stress–strain behavior of the different EPS materials is investigated by introducing all-around pressure on the EPS blocks that is equal to 50% of the vertical pressure. This pressure level was chosen to represent a typical at-rest condition that exists in granular material. The results of the analysis performed using the above material model are presented

Table 1 Properties of the backfill, geofoam and HSS structure used in the numerical model

Backfill soil properties					
Density (kg/m^3)	E (MPa)	ν Poisson's ratio	$\phi°$	$\psi°$	Cohesion (MPa)
1628	150	0.3	47	15	1E-5
EPS geofoam properties					
EPS material type			Density (kg/m^3)	E (MPa)	ν Poisson's ratio
EPS-39			38.4	17.8	0.15
EPS-22			21.6	6.91	0.1
EPS-15			14.4	4.20	0.1
Box material properties					
Square hollow section 250×250×10 mm			Density (kg/m^3)	E (GPa)	ν Poisson's ratio
–			7850	200	0.3
Interface parameters					
Interface type			Friction coefficient (μ)		E_{slip}
Soil-EPS			0.6		0.005
Soil-culvert			0.45		
EPS-culvert			0.3		

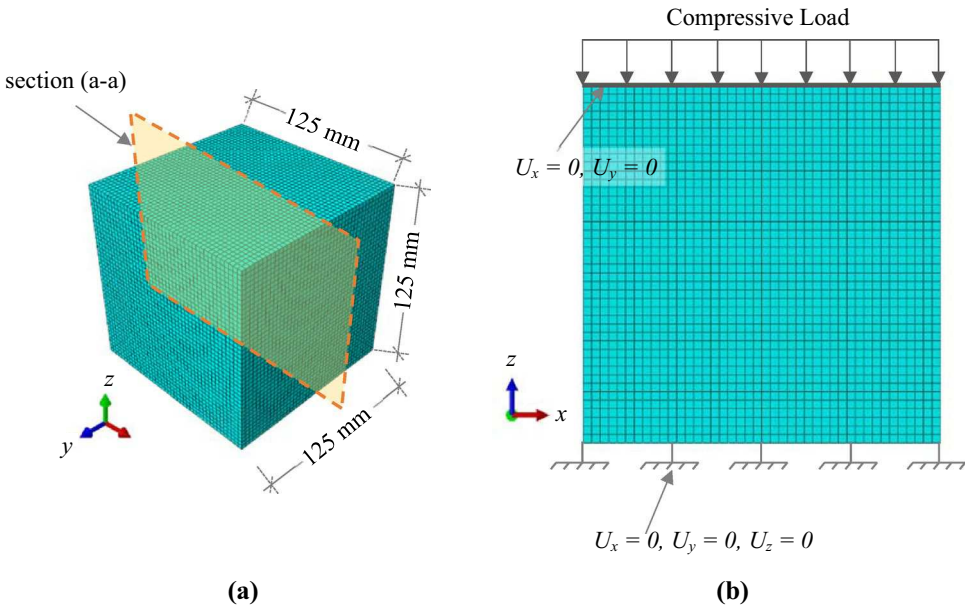

Fig. 4 FE model of the compression test: **a** 3D mesh, **b** 2D cross-section (a–a)

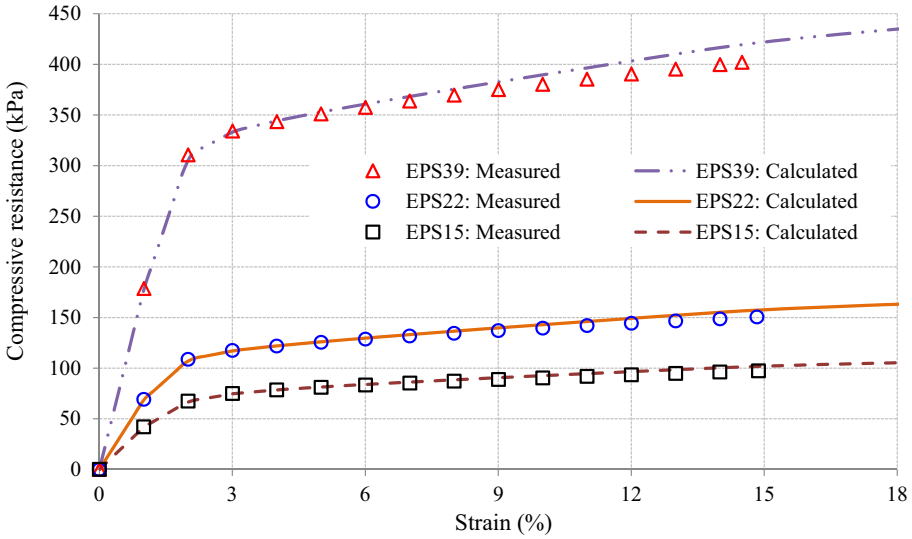

Fig. 5 Validation of the EPS material model

in Fig. 7. It can be seen that the EPS response is insensitive to confinement pressure up to about 2% strain. At high strain levels, the presence of confinement resulted in an increase in resistance to the applied axial load. For example, at 5% strain the confined EPS blocks (EPS15, EPS22 and EPS39) experienced an average increase in stress of about 12% as compared to the unconfined samples. It is therefore concluded that for the range of axial strains typically used in subsurface EPS geofoam application (1–5%), the confining pressure does not have a significant effect on the material response to axial loading.

Numerical Analysis of a Buried Structure Installed Using ITI Method

A two-dimensional finite element model has been developed to simulate the test setup shown in Fig. 8 and examine the role of EPS geofoam on the changes in earth pressure acting on a rigid buried structure. The setup consisted of a hollow structural section of 10 mm wall thickness instrumented using tactile pressure sensors [23–26]. A block of EPS geofoam, 2 inch in thickness, is used as a compressible material and placed directly above the structure. The chamber dimensions (1.4×1.2×0.45 m) are selected such that they represent two-dimensional loading condition. The

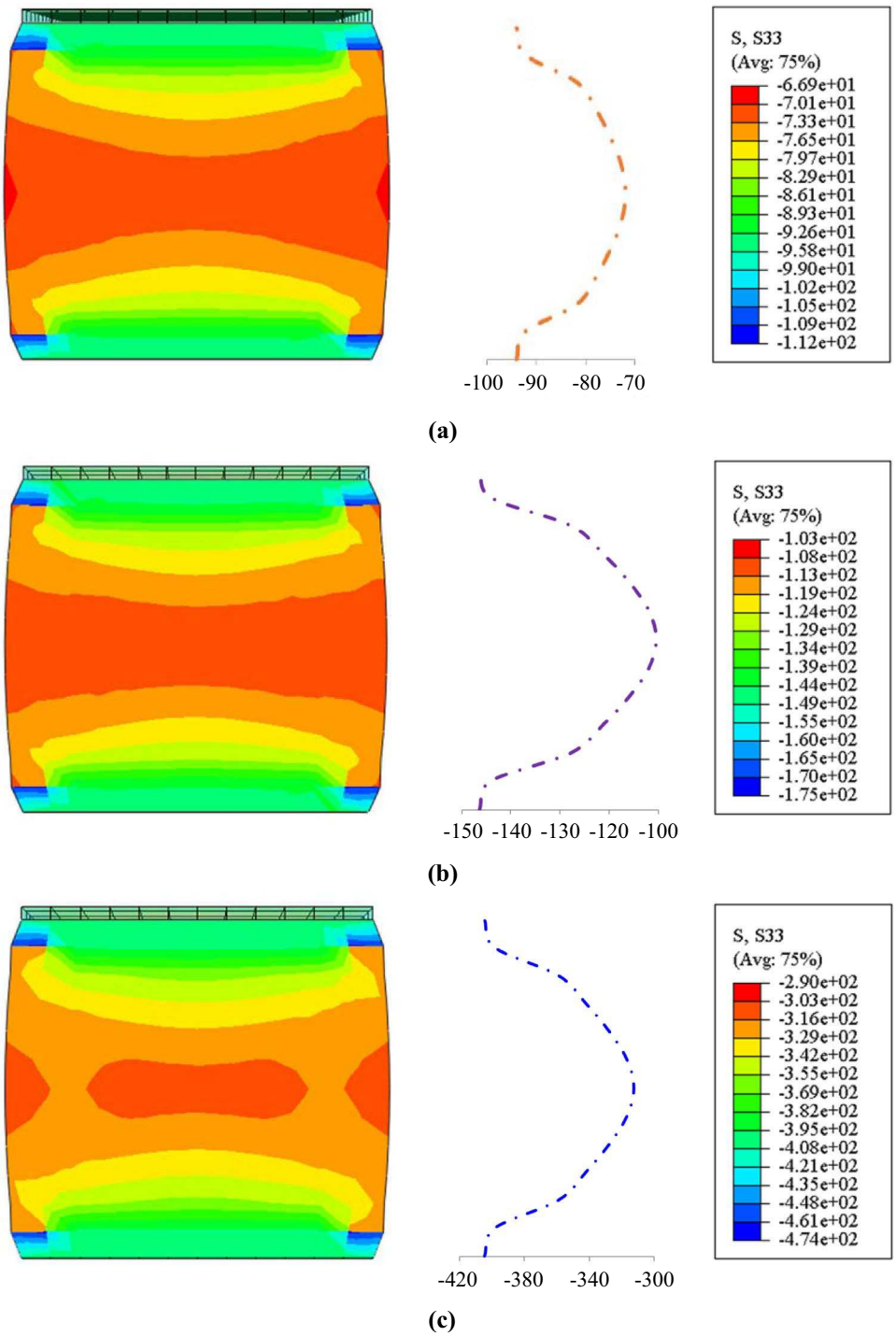

Fig. 6 Normal stress distribution (kPa) at 5% strain: **a** EPS15, **b** EPS22, **c** EPS39

use of air bag ensures uniform distribution of pressure on the surface of the soil. Dry sandy gravel with average unit weight of 16.3 kN/m^3 and friction angle of 47° is used as backfill material. A benchmark test is first conducted to measure the contact pressure on the walls of the structure due to the increase in surface pressure in the absence of geofoam. EPS geofoam blocks 5 cm (2 inch) in thickness, are then introduced immediately above the structure and the changes in contact pressure are measured for different geofoam densities. The details of the experimental investigation can be found elsewhere [27].

The finite element (FE) mesh that represents the geometry of the experiment, the boundary conditions, and the different soil zones around the HSS section is shown in Fig. 9. The mesh size was adjusted around the structure to provide sufficient resolution and accuracy

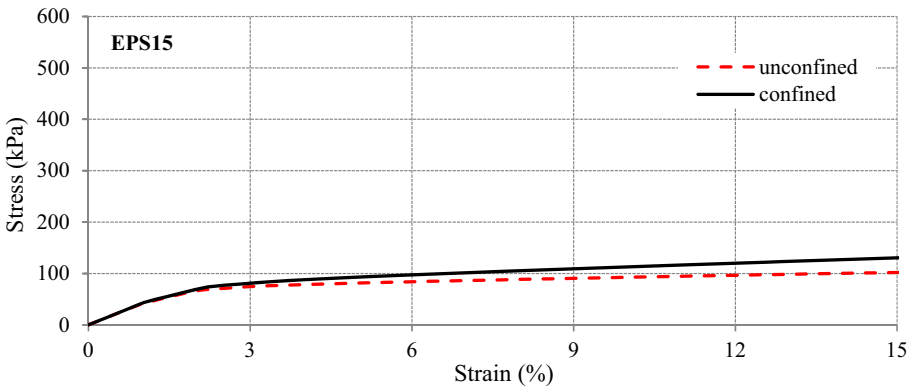

(a)

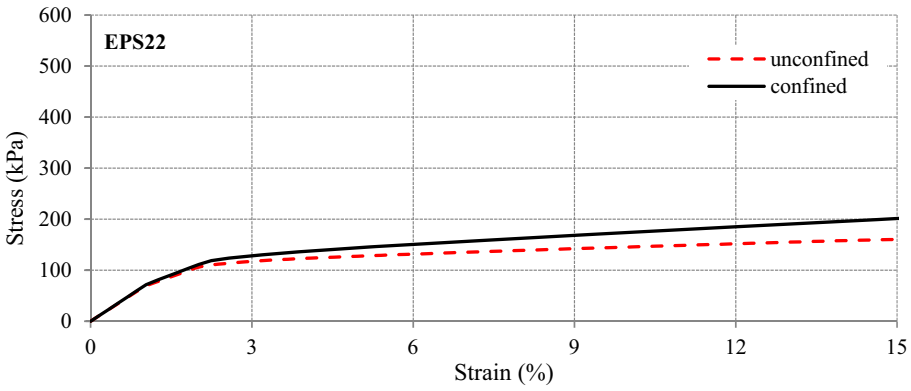

(b)

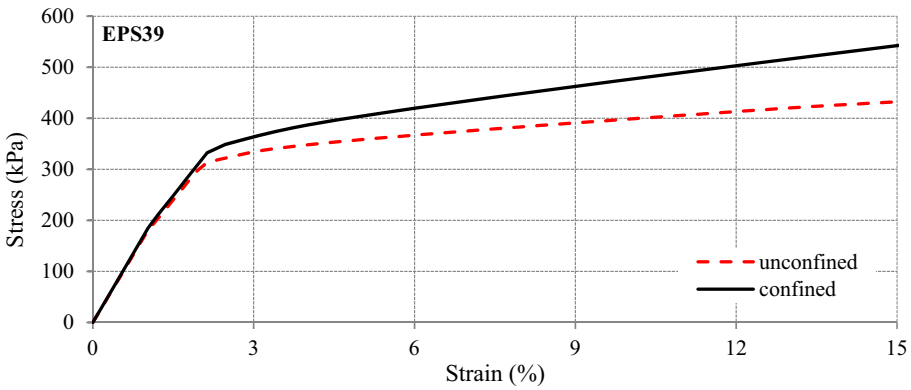

(c)

Fig. 7 Effect of confinement pressure on the stress–strain relationship of EPS material ($\sigma h = 0.5\ \sigma v$)

within the studied area. The complete mesh comprises a total of 1962 linear plane strain elements (CPE4) and 2282 nodes. Boundary conditions were defined such that nodes along the vertical boundaries may translate freely in the vertical direction but are fixed against displacements normal to the boundaries (smooth rigid). The nodes at the base are fixed against displacements in both directions (rough rigid).

Modeling Details

The backfill soil is modeled using elasto-plastic Mohr–Coulomb failure criteria with non-associated flow rule. The input parameters as listed in Table 1. The dilatancy angle was determined using Bolton's Equation [28] which relates the mobilized frictional angle (ϕ_p) to the critical state friction angle (ϕ_{cv}). The HSS section is treated as linear elastic material with density of 7850 kg/m^3, Poisson's ratio of 0.3, and Young's modulus of 200 GPa. The EPS material model developed

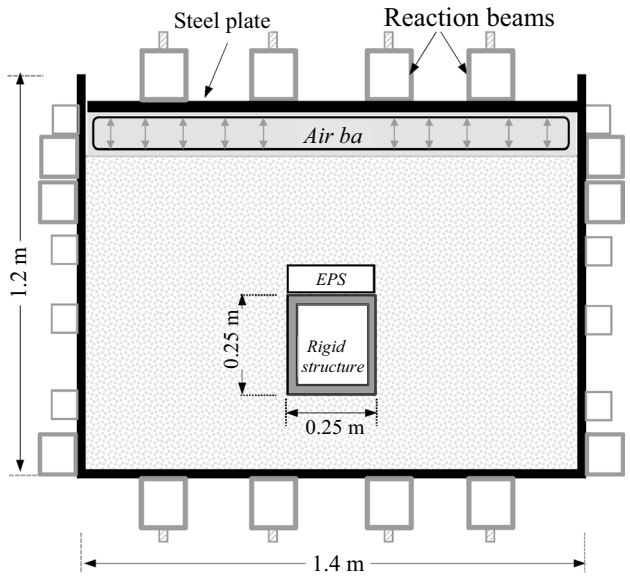

Fig. 8 Schematic of the modeled experimental setup

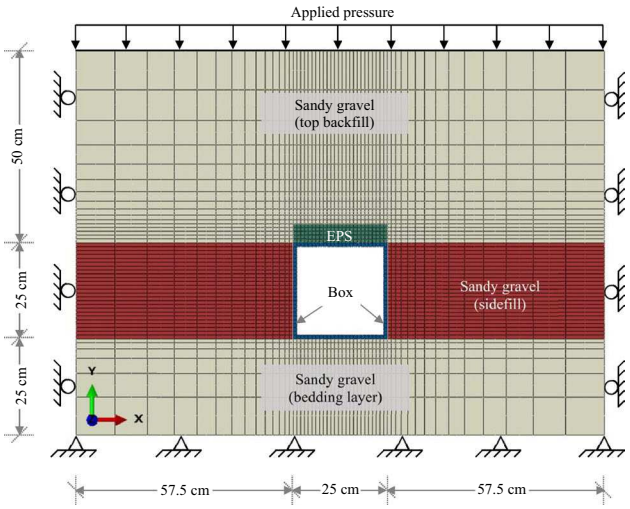

Fig. 9 The finite element mesh used in the analysis of the buried structure

in the previous section is used to simulate the geofoam inclusion.

Three different contact conditions are considered in this study; namely, (1) Soil-EPS interaction, (2) Soil-Structure interaction and (3) EPS-Structure interaction. These interactions are simulated using the surface-to-surface, master/slave contact technique available in ABAQUS. Contact formulation in 2D space covers both tangential and normal directions. In the tangential direction, Coulomb friction model is used to describe the shear interaction between the geofoam, the structure, and the surrounding soil. This model involves two material parameters- a friction coefficient (μ), and a tolerance parameter (E_{slip}). The shearing resistance (τ) is considered as a function of the shear displacement that represents the relative movement between the two contacted parties. On the other hand, a 'hard' contact model is used to simulate the contact pressure in the normal direction. The parameters used to describe these interface conditions are given in Table 1.

Calculated Versus Measured Earth Pressures

The numerical modeling results are first validated by comparing the calculated pressures on the walls of the buried structure with the measured values for the three cases (a) the benchmark test with no geofoam, (b) using EPS15, and (c) using EPS22. As shown in Fig. 10, the numerical model is able to capture the pressure changes, at the upper and lower walls of the structure, with a reasonable accuracy for the benchmark test as well as for the induced trench cases. Significant reduction in earth pressure was found due to the addition of EPS geofoam above the structure. For example, at surface pressure of 140 kPa, the earth pressure on the upper wall decreased by 60% (from 149 kPa for the benchmark case to 60 kPa) for the induced trench installation using EPS22 and the reduction in pressure reached about 70% (43 kPa) when EPS15 inclusion was introduced. Similar behavior was found at the lower wall with pressure reductions of 40% (90 kPa) and 45% (80 kPa) for EPS22 and 15, respectively.

Soil Arching Mechanism

To demonstrate the changes in pressure distribution on the walls of the buried structure, the in-plane principal stresses are presented in Fig. 11 at applied surface pressure of 140 kPa. When the box structure is buried in the backfill without geofoam inclusion (Fig. 11a), negative arching developed where the rigid box attracted more earth load compared to the surrounding soil. By examining the earth pressure distribution on a horizontal plane located along the top of the upper wall (Fig. 11a), it was found that the average pressure away from the influence zone of the buried structure is 144 kPa which increased to 149 kPa on the upper wall of the box. This represents the combined effect of the weight of the backfill material and the surface pressure applied at the top of the chamber. The contact pressure distribution dramatically changed when EPS15 block was placed immediately over the buried box as shown in Fig. 11b. The compression of the geofoam block created a reduction in contact pressure on the upper wall of the box (from an average of 149 to 43 kPa) coupled with an increase in pressure within the backfill material located on both sides of the box. The pressure distribution reveals that movement of the soil

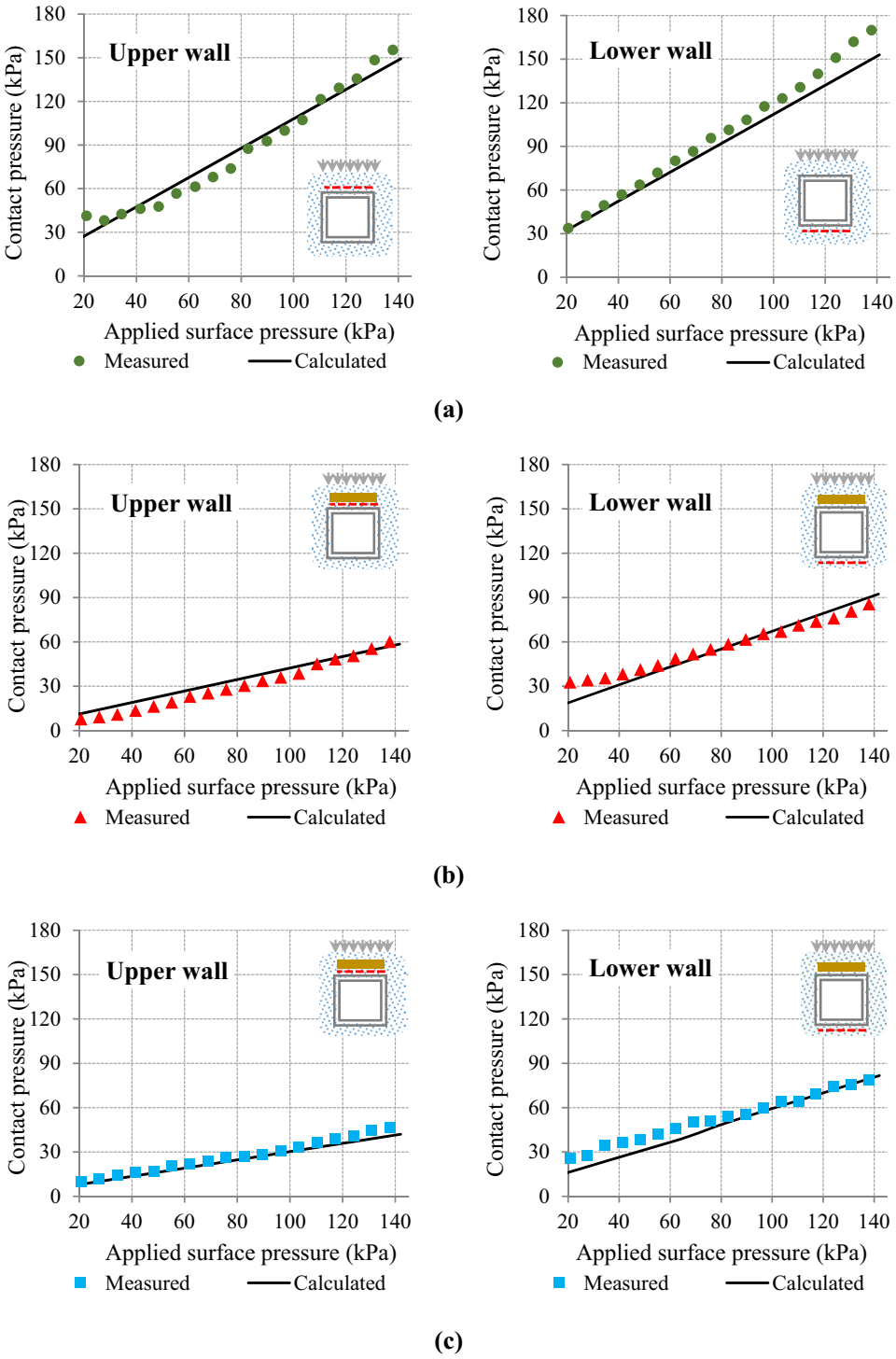

Fig. 10 Model validation for the cases of **a** no EPS, **b** EPS22 and **c** EPS15

column above the geofoam block resulted in not only in a contact pressure reduction on the upper wall but also a reduction in earth pressure above the box. By comparing the pressure distributions in Fig. 11, it is clear that induced trench installation using EPS geofoam has a significant impact of the earth loads transferred to the walls of the buried structure.

Effect of EPS Density

The effect of EPS density on the load transferred to the buried structure is numerically examined in this section by comparing the calculated pressures at the investigated locations (upper, lower and side walls) for three different EPS materials, namely, EPS15, EPS22, and EPS39. The

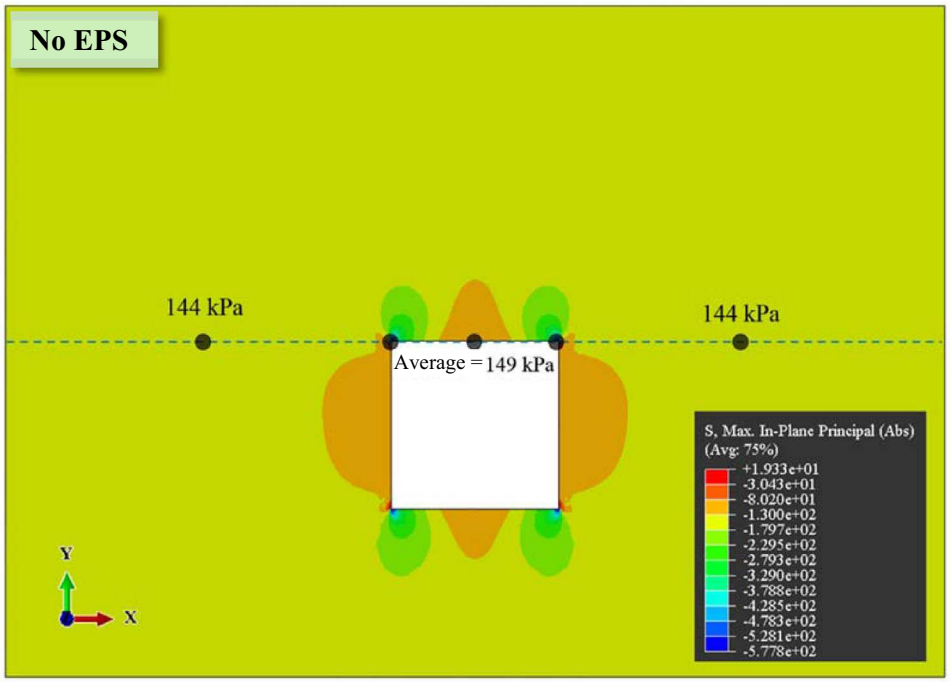

(a) No EPS geofoam

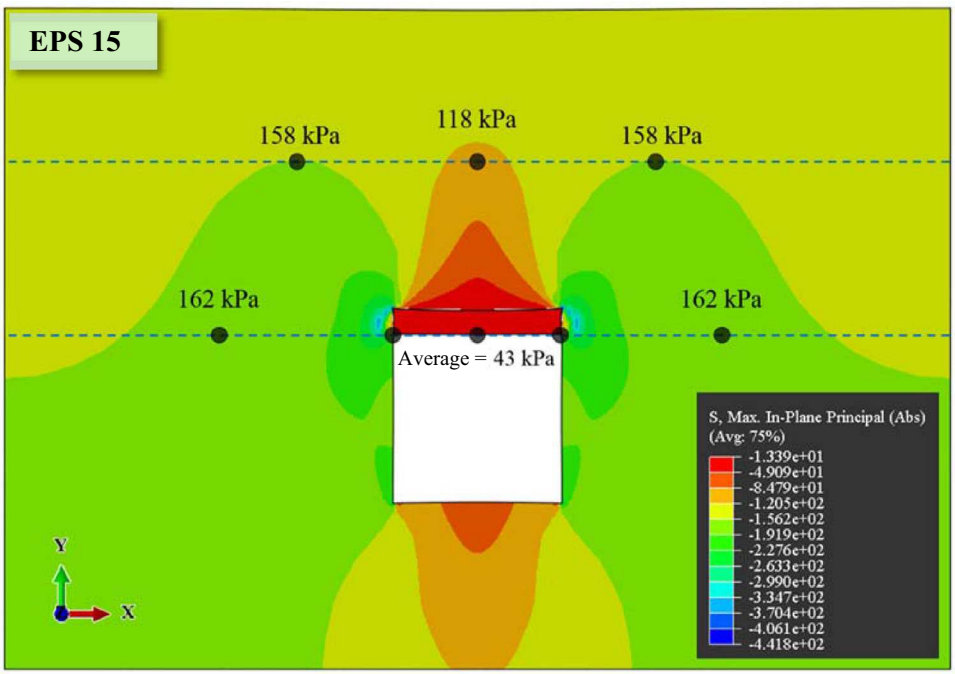

(b) EPS 15

Fig. 11 In-plane principal stress distribution around the structure at applied surface pressure of 140 kPa

maximum surface pressure was increased in the analysis up to 300 kPa to allow for the behavior of the system to be investigated at high stress levels. For the analyzed induced trench cases, the surface pressure that allows for a maximum of 1% strain in the EPS is used in this parametric study. The results are presented in Fig. 12a, b, c for the upper, lower and side walls, respectively. Contact pressure is also compared with the benchmark case (no EPS geofoam) to evaluate the effect of each EPS type on the load re-distribution around the buried structure. The vertical axes in Fig. 12 represent the contact pressure normalized with respect to that of the benchmark case.

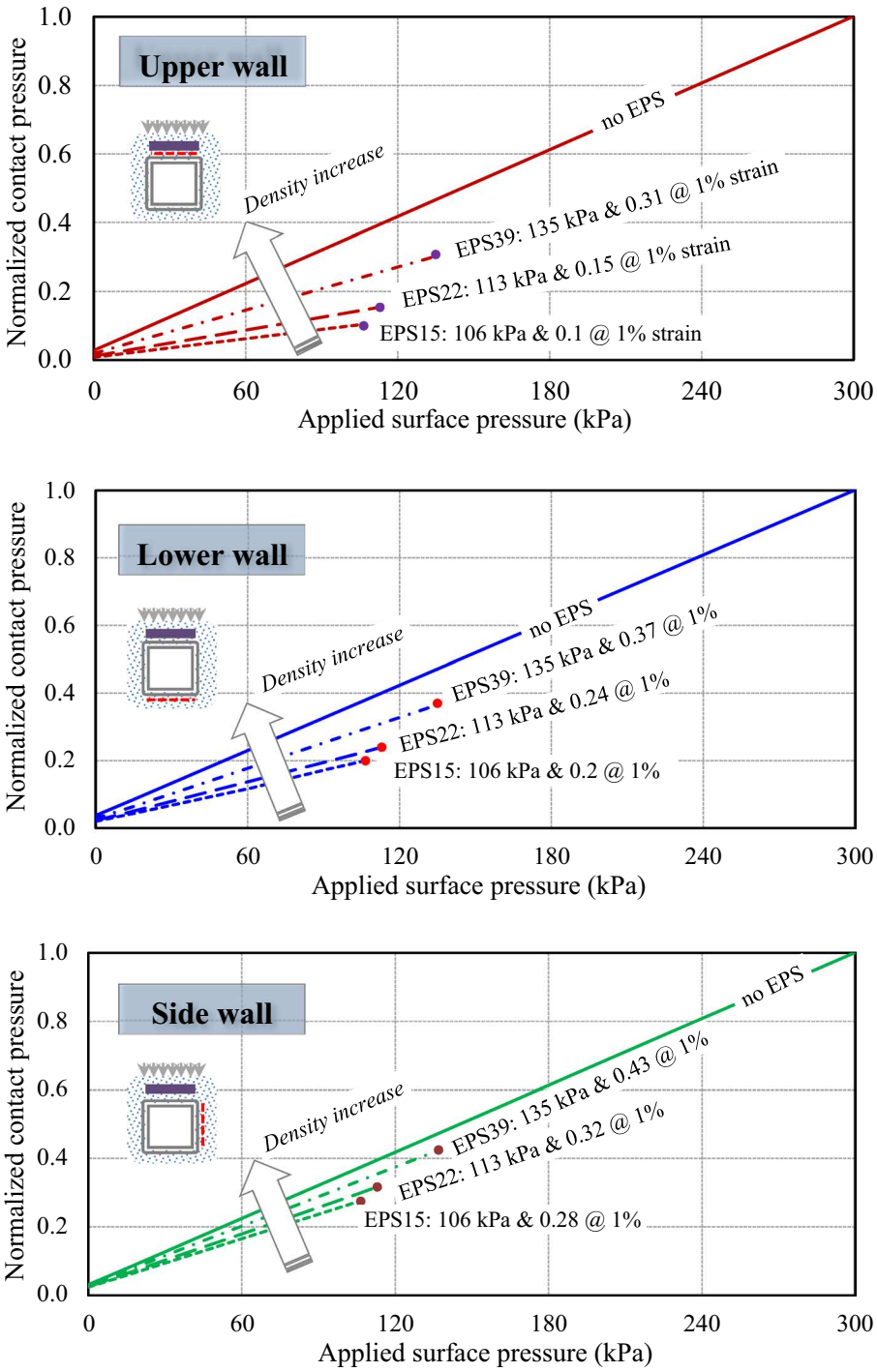

Fig. 12 Effect of EPS density on the earth pressure acting on the walls of the structure **a** upper wall, **b** lower wall, **c** side wall

For the upper wall (Fig. 12a), the EPS density was found to have a significant impact on the earth pressure acting on the wall. Compared with the benchmark, the lowest contact pressure is calculated for the case of EPS15 with pressure reduction of about 75% at an applied pressure of 105 kPa. The pressure reduction for EPS22 and EPS39 were found to be 60 and 30% at applied surface pressures of 113 and 135 kPa, respectively.

The pressure reduction ratios for the lower wall (Fig. 12b), at 1% strain, were found to be 47, 40 and 23% for EPS15, EPS22 and EPS39, respectively. These effects are found to be smaller compared to the reduction ratios calculated for the upper wall. Similar trends were found for the contact pressures on the side wall (Fig. 12c) with pressure reduction ratios of 25, 20 and 8%, respectively for the investigated EPS densities.

It is worth noting that, due to the linear nature of the calculated responses, the above reduction ratios are expected to apply for other EPS types and surface pressures as long as the maximum strain in the EPS does not exceed 1%.

Comparison with Theoretical Overburden Pressure

In this section, the earth pressures calculated using the numerical model is compared with the theoretical overburden pressure at different locations. Figure 13 shows the results for the upper, lower and side walls using three different types of EPS geofoams for up to a maximum fill height that corresponds to 1% strain in the geofoam block. The horizontal axis represents the fill height above the box which includes the effect of both the backfill material and the applied surface pressure. At the upper wall (Fig. 13a), the positive projecting case (no EPS) showed no difference from the theoretical overburden pressure γH (where H is

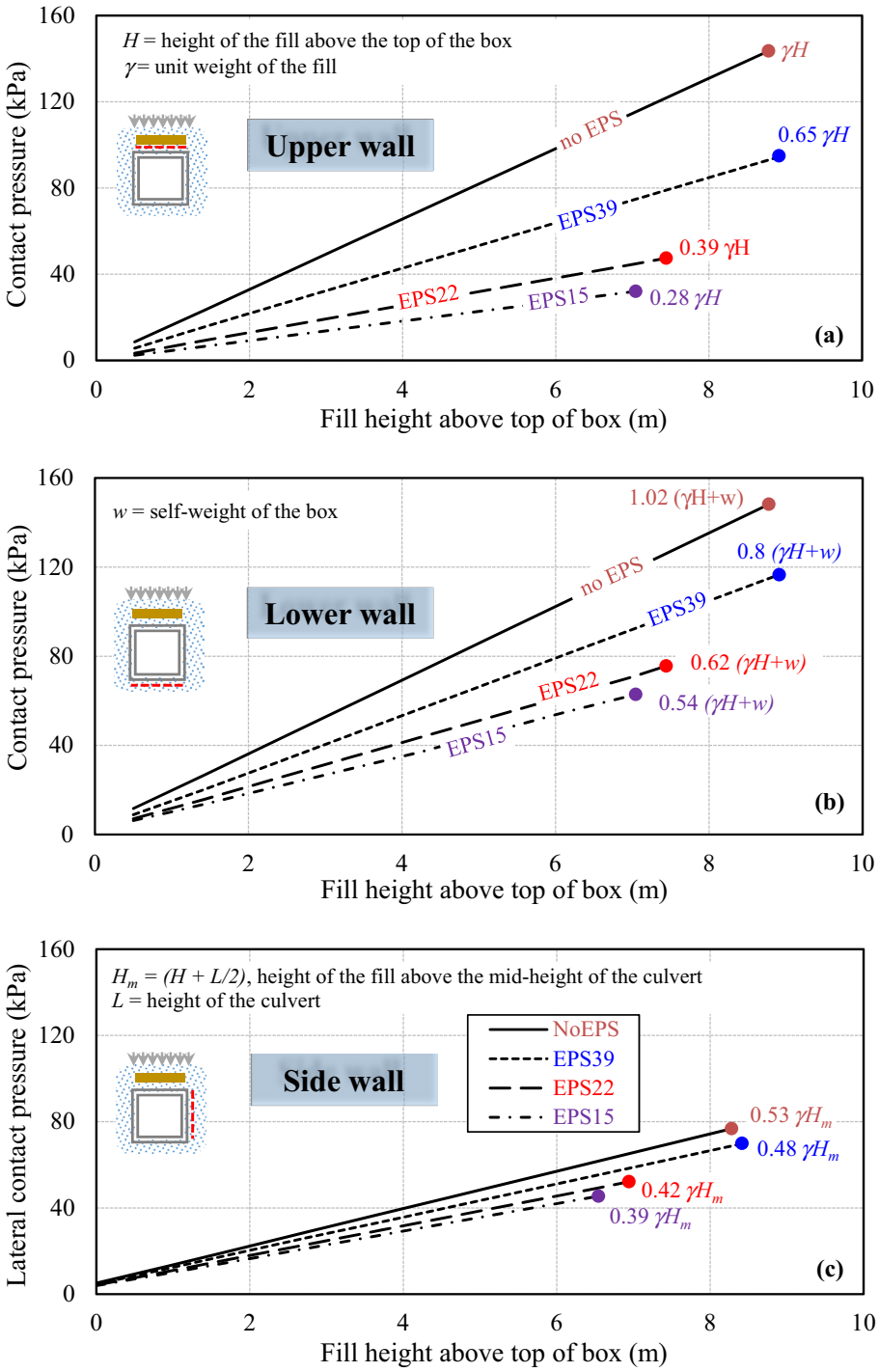

Fig. 13 Predicted contact pressures vs theoretical overburden pressures (*up* to 1% strain) for **a** upper wall; **b** lower wall; **c** sidewall

the height of the backfill above the upper wall and γ is the unit weight of the backfill). For the induced trench condition the calculated earth pressure values on the upper wall were found to be $0.65\gamma H$, $0.39\gamma H$ and $0.28\gamma H$ for EPS39, EPS22 and EPS15, respectively. These values correspond to pressure reductions of 35, 61 and 72% respectively.

The comparison between the predicted contact pressure at the lower wall and the theoretical overburden pressure (γH) plus the self-weight of the box (w) is presented in Fig. 11b. For the positive projecting case, the contact pressure at the lower wall was found to be 1.02 ($\gamma H + w$). Using EPS blocks, the calculated pressures were 0.8 ($\gamma H + w$), 0.62 ($\gamma H + w$) and 0.54 ($\gamma H + w$) for EPS39, EPS22 and EPS15, respectively.

The calculated lateral contact pressures on the side walls are compared with the theoretical overburden pressure at the mid-height of the box, γH_m (where $H_m = H + L/2$ and L is the vertical height of the box) as shown in Fig. 11c. For the positive projecting case, the calculated lateral pressure was found to be $0.53\gamma H_m$, while for the induced trench conditions the lateral pressure decreased to $0.48H_m$, $0.42H_m$, and $0.39H_m$ for EPS39, EPS22 and EPS15, respectively. These results suggest that careful selection of a suitable EPS geofoam density is important to ensure that earth pressure induced by a proposed embankment height to be built over a buried structure can be carried safely without exceeding the design strain limit of the geofoam material.

Summary and Conclusions

In this study, a numerical procedure for modeling the short-term response of EPS geofoam under uniaxial compression loading is developed using ABAQUS software. The model takes into account different features of the constitutive behavior responsible for the observed response in the laboratory, including material nonlinearity, plasticity and isotropic hardening. The material model is validated for three different EPS geofoam materials using index test results and the role of lateral confinement on the stress–strain response is also examined. Calibrated using the experimental data, a series of finite element analyses is performed to investigate the earth pressure distribution acting on a rigid buried structure installed using the induced trench method. The reduction in earth load on the structure is calculated for different EPS geofoam densities. Results showed that the introduction of EPS geofoam block immediately above the structure has a significant effect on the contact pressure distribution particularly on the upper wall covered by the geofoam inclusion.

The calculated pressures on the buried box were compared to the theoretical overburden pressures (resulting from the self-weight of the soil) in addition to the external surface loading. It is found that significant pressure reduction is achieved using EPS15 with a pressure ratio of 0.28 of the theoretical overburden pressure at the upper wall. This translates into a reduction in contact pressure of about 70% on the upper wall.

Finally, the proposed FE modeling approach has proven to be efficient in capturing the behavior of EPS geofoam material under complex interaction soil-structure condition and can be adopted to simulate similar soil-geofoam-structure interaction problems.

Acknowledgements This research is supported by the Natural Sciences and Engineering Research Council of Canada (NSERC) CRD project No. 452760-13. The generous support of Plasti-Fab Ltd. throughout this study is appreciated.

References

1. Canadian Standards Association (CSA) (2006) Canadian highway bridge design code, Canadian Standards Association (CSA), Mississauga
2. AASHTO (2012) LRFD bridge design specifications, 6th edn. American Association of State Highway and Transportation Officials, Washington, D.C.
3. McAffee RP, Valsangkar AJ (2008) Field performance, centrifuge testing, and numerical modelling of an induced trench installation. Can Geotech J 45:85–101
4. Sladen JA, Oswell JM (1988) The induced trench method—a critical review and case history. Can Geotech J 25:541–549
5. Vaslestad J, Johansen TH, Holm W (1993) Load reduction on rigid culverts beneath high fills: long-term behavior. Transp Res Rec 1415:58–68
6. Liedberg NSD (1997) Load reduction on a rigid pipe: pilot study of a soft cushion installation. Transp Res Record
7. Sun L, Hopkins T, Beckham T (2011) Long-term monitoring of culvert load reduction using an imperfect ditch backfilled with Geofoam. Transp Res Record 2212:56–64
8. Oshati OS, Valsangkar AJ, Schriver AB (2012) Earth pressures exerted on an induced trench cast-in-place double-cell rectangular box culvert. Can Geotech J 49:1267–1284
9. Kim K, Yoo CH (2002) Design Loading for deeply buried box culverts. Highway Research Center, Auburn University, Report No. IR-02-03., Alabama, USA, p 215
10. Kang J, Parker F, Kang YJ, Yoo CH (2008) Effects of frictional forces acting on sidewalls of buried box culverts. Int J Numer Anal Methods Geomech 32:289–306
11. Sun L, Hopkins TC, Beckham TL (2009) Reduction of stresses on buried rigid highway structures using the imperfect ditch method and expanded polysterene (geofoam) Kentucky Transportaion Center, University of Kentucky, Report No. KTC-07-14-SPR-228-01-1F, Kentucky, USA, p 49
12. McGuigan BL, Valsangkar AJ (2010) Centrifuge testing and numerical analysis of box culverts installed in induced trenches. Can Geotech J 47:147–163
13. McGuigan BL, Valsangkar AJ (2011) Earth pressures on twin positive projecting and induced trench box culverts under high embankments. Can Geotech J 48:173–185
14. Horvath JS (2001) Concepts for cellular geosynthetics standards with example for EPS-block geofoam as lightweight fill for roads. Manhattan College Research Report No. CGT-2001–4, USA

15. Takahara T, Miura K (1998) Mechanical characteristics of EPS block fill and its simulation by DEM and FEM. Soils Found 38(1):97–110
16. Hazarika H (2006) Stress–Strain modeling of EPS Geofoam for large-strain applications. Geotext Geomembr 24(2):79–90
17. Chun BS, Lim HS, Sagong M, Kim K (2004) Development of a hyperbolic constitutive model for expanded polystyrene (EPS) geofoam under triaxial compression test. Geotext Geomembr 22(4):223–237
18. Leo CJ, Kumruzzaman M, Wong H, Yin JH (2008) Behavior of EPS geofoam in true triaxial compression tests. Geotext Geomembr 26(2):175–180
19. Ekanayake SD, Liyanapathirana DS, Leo CJ (2015) Numerical simulation of EPS geofoam behaviour in triaxial tests. Eng Comput 32(5):1372–1390
20. ASTM D16210-10—Standard Test Method for Compressive Properties of Rigid Celleular Plastics
21. ABAQUS (2013) ABAQUS User's Manuals, Version 6.13, Dassault Systems Simulia Corp., Providence, RI, USA
22. Negussey D (2007) Design parameters for EPS geofoam. Soils Found 47(1):161–170
23. Ahmed M, Tran V, Meguid MA (2015) On the role of geogrid reinforcement in reducing earth pressures on buried pipes. Soils Found 5(33):588–599
24. Ahmed MR, Meguid MA, Whalen J (2013) Laboratory Measurement of the Load Reduction on Buried Structures overlain by EPS Geofoam, The 66th Canadian Geotechnical Conference, Montreal, Canada, Paper No. 217 p 8
25. Hussein MG, Meguid MA (2015) Numerical modeling of soil-structure interaction with applications to geosynthetics. International Conference on Structural and Geotechnical Engineering, Ain Shams University, December, Cairo, Egypt, p 12
26. Hussein MG, Meguid MA, Whalen J (2015) On the numerical modeling of buried structures with compressible inclusion, GeoQuebec, September, Quebec City, p 8
27. Ahmed MR (2016) Experimental investigations into the role of geosynthetic inclusions on the earth pressure acting on buried structures. PhD. Thesis, Civil Engineering and Applied Mechanics. McGill University, Canada
28. Bolton MD (1986) The strength and dilatancy of sands. Géotech 36(1):65–78